Journal of Heat and Mass Transfer Research 10 (2023) 147 - 158

Journal of Heat and Mass Transfer Research

Journal homepage: https://jhmtr.semnan.ac.ir

Semnan University

Research Article

Numerical Study on Thermo-Hydraulic Performances of Hybrid Nanofluids Flowing through a Corrugated Channel with Metal Foam

Moslem Abrofarakh, Hamid Moghadam *

Department of Chemical Engineering, University of Sistan and Baluchestan, Zahedan, Iran

PAPER INFO

Paper history:

Received: 2022-10-27
Revised: 2023-10-02
Accepted: 2023-10-03

Keywords:

Heat transfer;

Metal foam;

Hybrid nanofluids;

CFD.

ABSTRACT

In this study, a novel design was proposed for enhancing heat transfer in a channel with metal foam, corrugated walls, and hybrid nanofluids. The numerical analysis of hybrid nanofluids (MWCNTs+TiO_2) with DW (distillate water) as the base fluid was performed in a channel with triangular corrugations and open metal foam. The mass fractions of hybrid nanofluids (mixture of DW and MWCNTs+TiO_2) were set at 0.025%, 0.05%, and 0.075%. The effects of metal foam porosity and PPI (pore density), as well as different Reynolds numbers (ranging from 7000 to 13000), on thermal performance were investigated. The results showed that the heat transfer enhancement with metal foam increased by 130% for all hybrid nanofluids. Moreover, the heat transfer enhancement in metal foam with a porosity of 0.9 was 9.8% higher than that of metal foam with a porosity of 0.99. Additionally, quadratic correlations for the average Nusselt number (Nu_a) were proposed for all hybrid nanofluids, taking into account PPI, porosity, and Reynolds numbers as variables. Finally, the optimum values of Nu_a for all hybrid nanofluids were determined, providing valuable insights for optimizing the heat transfer performance in this configuration.

DOI: 10.22075/jhmtr.2023.28829.1400

1. Introduction

Heat transfer is an important issue for several industries such as power plants, refineries, petrochemicals, biological systems, and electronic components [1,2,3]. Numerous studies in the field of heat transfer enhancement have been carried out in the last two decades. In recent years, studies on heat transfer with metal foams, nanofluids, and corrugated channels have gained significant attention due to their increased heat transfer rate [4]. An experimental investigation of a channel with metal foam and oscillating flow was provided in the study of Leong [5]. The results highlighted that the use of metal foam and oscillation flow increase the Nusselt number. An analytical study of the heat transfer on a pipe, filled with metal foam was provided by Lua, et al. [6]. The results showed that porosity and pore size are important parameters of metal foam. Yu et al. examined the effects of pore size and porosity on the performance of a carbon-foam finned tube heat exchanger [7]. According to the results obtained, metal foam improved thermal performance by approximately 15%. A simulation of the metal hydride reactor was conducted by Laurencelle and Goyette [8], which showed good agreement between the model and the experimental data when using metal foam. Du et al. provided a numerical analysis of heat transfer in a metal foam-filled heat exchanger [9]. The results showed that the proposed numerical model effectively

* *Corresponding Author: Hamid Moghadam.*
Email: h.moghadam@eng.usb.ac.ir

represented the real physical heat transfer process in the double-pipe heat exchanger. In the work of Khadangi et al. [10], an experimental investigation of a vertical cylinder using non-Newtonian nanofluids was conducted. The results indicated that heat transfer performance with nanofluids improved at low concentrations. Su et al. [11] conducted an experimental investigation of the effects of nanoparticles on the physical properties of a binary nanofluid and proposed a correlation for the effective thermal conductivity of the nanofluid. Yu et al. [12] conducted an experimental study of convective heat transfer using polyalphaolefin nanofluids. The results indicated that a proper interpretation of the experimental data of nanofluids containing non-spherical nanoparticles in convective flow required consideration of shear-induced alignment and orientational motion of the particles. In their study, Perarasu et al. conducted experimental investigations of heat transfer with nanofluids in a coiled agitated vessel [13]. The results highlighted a 17.59% improvement in heat transfer. Ijame et al. [14] provided a mini-channel experiment with TiO2-water nanofluid and SiC-water nanofluid, showing a 12.43% improvement in heat transfer. Another experimental study was performed to investigate the thermal performance of a heat pipe with an inclined mesh, and the results indicated that an inclination angle of 45° yielded the best results [15]. Numerous experimental studies were conducted to investigate the thermal performance of various nanofluid configurations and geometries [16,17,18,19,20]. Zachár et al. [21] conducted a numerical investigation of heat transfer in a heat exchanger with helical corrugations, and the results indicated a 100% improvement in heat transfer. Hikmet et al. [22] studied the characteristics of Al2O3-water flow inside a corrugated channel. The results indicated an improvement in the performance of heat transfer. Zahrana et al. [23] conducted both numerical and experimental investigations of airflow through a rectangular channel with one corrugated surface. The results highlighted that the presence of a corrugated surface enhanced the heat transfer rate. Obaidia et al. conducted a study where different corrugated geometrical configurations were used to investigate Nusselt numbers [24]. In a study by Amrar et al., friction factors and Nusselt numbers in an annular corrugated channel were investigated, and the results indicated that the heat transfer area could be reduced by up to 30–65% [25]. Feng et al. studied a corrugated triangular flow channel with trapezoidal baffles, and the results showed that the friction factor and Nusselt number were more than 3.5 and 1.7 times higher, respectively, than those without baffles [26]. Li et al. conducted a study proposing the enhancement of heat transfer efficiency using a piezoelectric fan on corrugated surfaces, and the results demonstrated improved heat transfer [27]. Lia et al. investigated heat transfer in helical tubes with spherical corrugations and proposed a pulsating flow. The results indicated that both the friction factor and Nusselt number increased with an increase in dimensionless amplitude [28]. Talib et al. conducted a study on fluid flow and heat transfer through backward-facing steps, which was investigated experimentally and numerically. The results showed that the corrugated wall increased the friction factor and Nusselt number by up to 46.2% and 40.7%, respectively [29]. Hu et al. studied three corrugated tubes proposed for enhancing the heat transfer rate of the intermediate heat exchanger [30]. Li et al. investigated a corrugated heat storage system with porous metal [31]. Bianco et al. studied a confined channel with nanofluids and metal foam [32]. Wan et al. conducted an experimental study investigating the effects of TiO2-water nanofluids and copper foam on heat transfer in a corrugated tube [33]. Many studies to enhance heat transfer have been reported in the literature. In most of the studies, the effect of the nanofluid, corrugated wall, and metal foam or combination of two of these techniques has been investigated. Based on the studies reviewed above, there has been no study on improving heat transfer in a channel with simultaneous use of corrugated wall, metal foam, and hybrid nanofluids. In this study, a novel design for enhancing heat transfer in a channel with metal foam, corrugated walls, and hybrid nanofluids was proposed. The effects of porosity, pore density, and weight concentrations of nanofluids on heat transfer behaviors in the rectangular channel with triangular corrugations were numerically examined.

2. Geometrical and Physical model

In Figure 1, a rectangular channel with triangular corrugations is depicted without metal foam. The protruded surface has a length of 100 mm, the channel's height is 30 mm, and there are 5 mm between the vertical distances of the corrugation teeth [34].

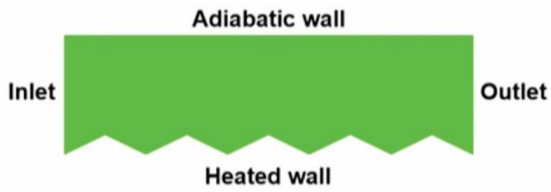

Figure 1. Computational domain of the rectangular channel without metal foam [34]

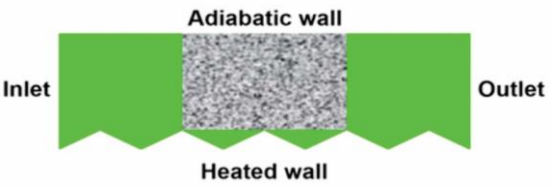

Figure 2. Computational domain of the rectangular channel with metal foam

In Figure 2, the rectangular channel features triangular corrugations and Aluminum metal foam. The metal foam has dimensions of 40 mm in length and 25 mm in width. In the current numerical investigation, the flow of hybrid nanofluids is assumed to be turbulent, steady-state, two-dimensional, Newtonian, incompressible, and single-phase. Within the metal foam zone, local thermal non-equilibrium (LTNE) conditions between the solid and nanofluid temperatures are considered. Physical properties are assumed to be constant, and viscous dissipation is considered negligible.

3. Governing Equations

Based on the physical model assumptions, the equations of continuity, momentum, and energy in this research are as follows [32, 35, 36]:

Continuity

$$\nabla.\boldsymbol{u} = 0 \tag{1}$$

Momentum

$$\rho(\boldsymbol{u}.\nabla)\boldsymbol{u} = \nabla.[-pI + K] \tag{2}$$

$$K = (\mu + \mu_T)(\nabla\boldsymbol{u} + (\nabla\boldsymbol{u})^T) \tag{3}$$

Momentum (metal foam)

$$\frac{1}{\varepsilon_p^2}(\rho(\boldsymbol{u}.\nabla)\boldsymbol{u}) = \nabla.[-pI + K] - \left(\frac{\mu}{\kappa} + \beta\rho|\boldsymbol{u}|\right)\boldsymbol{u} \tag{4}$$

$$K = \frac{\mu}{\varepsilon_p}(\nabla\boldsymbol{u} + (\nabla\boldsymbol{u})^T) - \frac{\mathbf{2}}{\mathbf{3}}\frac{\mu}{\varepsilon_p}(\nabla.\boldsymbol{u})\boldsymbol{I} \tag{5}$$

$$\kappa = \frac{d_p^2\left(1-(1-\varepsilon_p)^{\frac{1}{3}}\right)}{108\left(\left(1-\varepsilon_p\right)^{\frac{1}{3}} - \left(1-\varepsilon_p\right)\right)} \tag{6}$$

$$\beta = \frac{0.55}{\sqrt{\kappa}} \tag{7}$$

Turbulent kinetic energy

$$\rho(\boldsymbol{u}.\nabla)k = \nabla.[\left(\mu + \frac{\mu_T}{\sigma_k}\right)\nabla k + p_k - \rho\varepsilon \tag{8}$$

Turbulent dissipation rate

$$\rho(\boldsymbol{u}.\nabla)\boldsymbol{\varepsilon} = \nabla.[\left(\mu + \frac{\mu_T}{\sigma_k}\right)\nabla\boldsymbol{\varepsilon} + \frac{C_{\varepsilon_1}\varepsilon}{k}p_k - \frac{C_{\varepsilon_2}\varepsilon^2\rho}{k} \tag{9}$$

Energy (nanofluids)

$$\rho c_p\boldsymbol{u}.\nabla T + \nabla.\boldsymbol{q} = 0 \tag{10}$$

$$\boldsymbol{q} = -k.\nabla T \tag{11}$$

Energy (metal foam)

$$\rho c_p\boldsymbol{u}.\nabla T + \nabla.q = Q \text{ (fluid)} \tag{12}$$

$$q = -\varepsilon_p k_{nf}.\nabla T_{nf} \tag{13}$$

$$Q = h_a(T_S - T_{nf}) \tag{14}$$

$$\nabla.q_S = -Q \text{ (Solid)} \tag{15}$$

$$q_S = -(1-\varepsilon_p)k_s.\nabla T_S \tag{16}$$

$$h_a = ah \tag{17}$$

$$h = 0.26Re^{0.6}Pr^{0.37}\left(\frac{k_{nf}}{d_f}\right) \tag{18}$$

$$Re = \frac{\rho\boldsymbol{u}d}{\mu} \tag{19}$$

$$Pr = \frac{\mu cp_{nf}}{k_{nf}} \tag{20}$$

$$Nu = \frac{h_{av}d}{k_{nf}} \tag{21}$$

$$h_{av} = \frac{q''}{T - T_b} \tag{22}$$

$$a = \frac{3\pi d_f}{\left(0.50d_p\right)^2}\left(1 - e^{-\frac{(1-\varepsilon_p)}{0.04}}\right) \tag{23}$$

where, $\mathbf{u}$ is the velocity, p is the pressure, μ is the viscosity, ε_p is porosity, $\boldsymbol{\kappa}$ is permeability, cp is specific heat capacity, ks and k_{nf} are the thermal conductivity of the solid and nanofluids, T_s and T_{nf} are the temperature of the solid and nanofluids, respectively. In equations (22) and (18), h and a are the interfacial heat transfer coefficient between the solid and nanofluids specific surface area density, respectively. Boundary conductions in this study are shown in Table 1 [34].

Table1. Boundary conditions of this study

Boundary conduction	Fluid flow	Heat transfer
Inlet	u= ui, v=0	T=303 K
Outlet	p = 0	-n.q=0
Adiabatic wall	No slip	-n.q=0
Corrugated wall	No Slip	T= 311 K

4. Numerical Model

The equations of continuity, momentum, turbulent (k-ε), and energy for nanofluid and metal foam, along with the physical properties listed in Table 2 and boundary conditions outlined in Table 1, were numerically solved using the finite element method in COMSOL Multiphysics (V.6).

Table 2. Physical properties of the base fluid (DW) and hybrid nanofluids in different weight concentrations [34]

Physical properties	DW	0.025 %-wt	0.05%-wt	0.075 %-wt
ρ(kg/m³)	995.652	1014.139	1032.95	1052.473
C_P (J/ (kg. K))	4180	4068.9	4067.18	4064.8
k (W/ (m.K))	0.616	0.689118	0.717553	0.733566
μ (Pa. s)	0.797	0.927	0.980	1.039

The physical properties of DW and hybrid nanofluids (MT) with concentrations of 0.025%-wt, 0.050%-wt, and 0.075%-wt are listed in Table 3 [34]. The study covers a range of porosity from 0.9 to 0.99 and pore density from 20 to 40.

For grid verification analysis, various grid sizes were employed, and the results were compared with the Nusselt number obtained from the Dittus-Boelter equation (Eq. 23).

$$Nu=0.023\ Re^{0.8}\ Pr^{0.4} \quad (23)$$

Figure 4 illustrates the Nusselt number obtained from the model and the Dittus-Boelter equation for three different mesh sizes. The average relative error between mesh 2 (9300) and mesh 3 (14500) is 1.8%. Additionally, the average relative errors for mesh 1 (9300), mesh 2, and mesh 3 when compared to the Dittus-Boelter equation are 19.4%, 9.1%, and 7.4%, respectively.

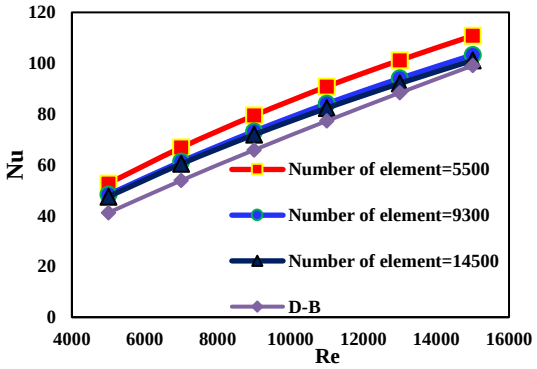

Figure 3. Verification of grids with three meshes

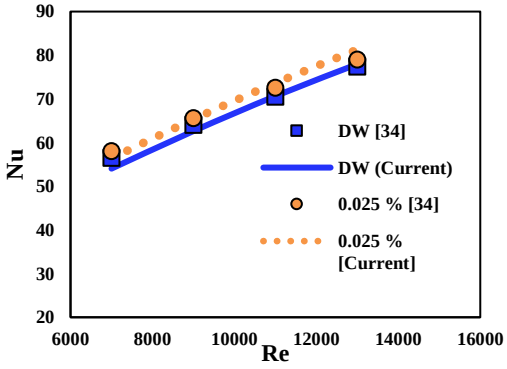

Figure 4. Validation of the model with [34] data

To validate the model without metal foam, the Nua for different mass concentrations of nanofluids was compared with the data presented by Alawi et al. [34]. The results indicate an average relative error of only 1.3%, demonstrating reasonable agreement between the current model and the data from Alawi et al. To validate the model with metal foam, experimental data from Kamath et al. [37] was utilized, and a comparison of pressure drops between the model and experimental data is shown in Figures 5. The maximum relative error in pressure drop is 4%, while the average relative error is 2.1%. These results demonstrate significant consistency between the experimental data and the present model.

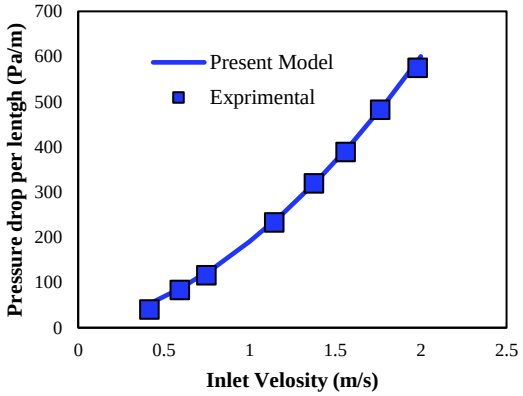

Figure 5. Validation of the model with [38] data

5. Results and Discussions

Figures 6 and 7 show the velocity and pressure profiles for distilled water (without nanofluid) and MT (nanofluid with 0.075 wt %) with metal foam (ε=0.99, PPI=40) and without foam. The pressure drop of MT with metal foam or without metal foam is more than DW, since the viscosity of MT is higher than DW. When there is the metal foam in the channel, the maximum velocity has increased in both MT and DW states, its due to the pressure drop of adding metal foam. As a result, both convective and conductive heat transfer in the channel with metal foam increase due to its higher thermal conductivity and increased velocity. The higher velocity contributes to a reduction in thermal resistance at the bottom of the rectangular channel. Furthermore, Figure 6 clearly illustrates that the utilization of metal foam has resulted in a more uniform velocity profile within the flow channel.

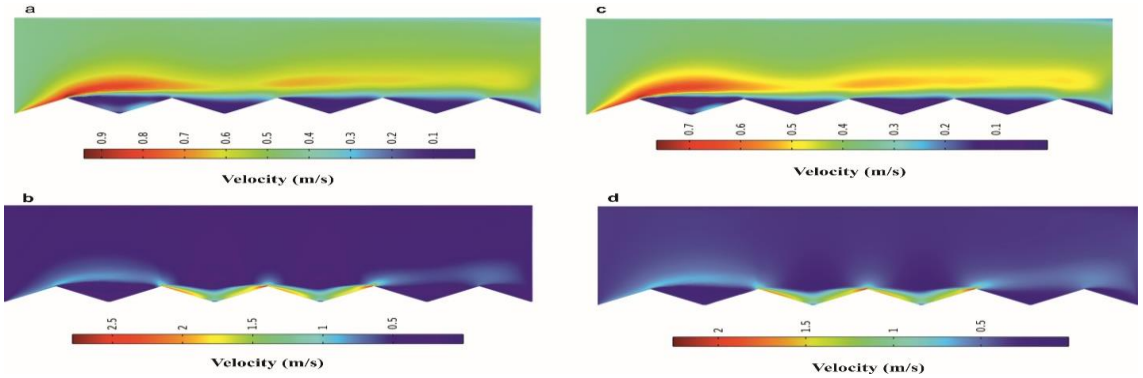

Figure 6. Profiles of velocity, a: nanofluid (0.075 %) without metal foam, b: nanofluid (0.075 %) with metal foam, c: DW without metal foam, d: DW with metal foam

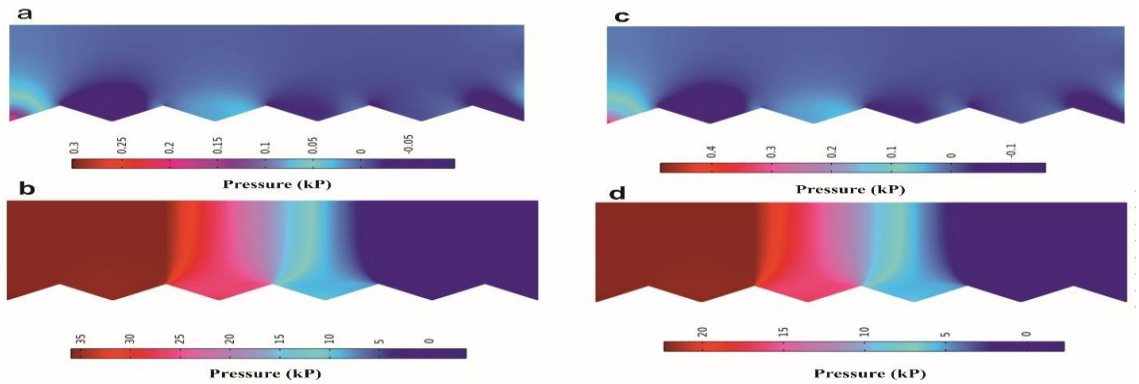

Figure 7. Profiles of pressure, a: nanofluid (0.075 %) without metal foam, b: nanofluid (0.075 %) with metal foam, c: DW without metal foam, d: DW with metal foam

In Fig. 8, the Nua is presented for different mass fraction of nanofluids, with metal foam (ε=0.9, PPI=20) and without metal foam. The Nua of nanofluids in the metal foam are 130 % higher than without metal foam. This increasing is due to high thermal conductivity of the metal foam and decrease the thermal resistance in bottom of rectangle channel. Also, this Figure shows the Nua of MT (0.075 %) is 2.54 % higher than DW.

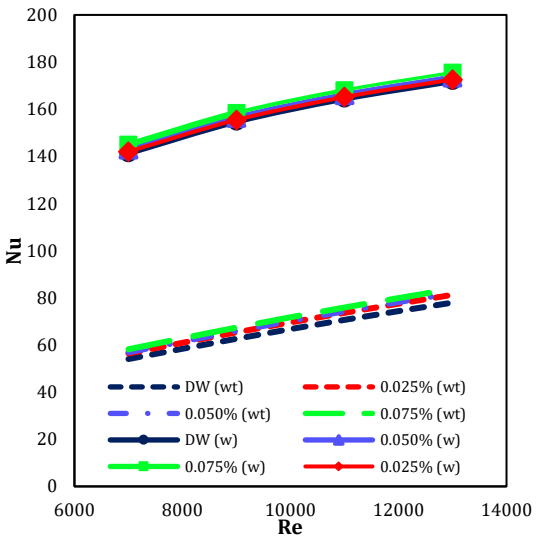

Figure 8. Nu_a as function of Reynolds number for different nanofluids mass fraction

In Figure 9, the pressure drops of the channel with metal foam are presented for different mass fractions of nanofluids, two values of porosity, and a pore density of 20 PPI. The values of porosity are 0.9 (Figure 9-a) and 0.99 (Figure 9-b). The pressure drops of the channel with a porosity of 0.9 are higher than those of the channel with 0.99 porosity. This difference is attributed to the fact that a higher porosity allows for a larger cross-sectional area of fluid flow, resulting in smaller pressure drops. Additionally, the pressure drops of nanofluid with a 0.075% mass fraction are higher than those of the other nanofluids due to its higher viscosity.

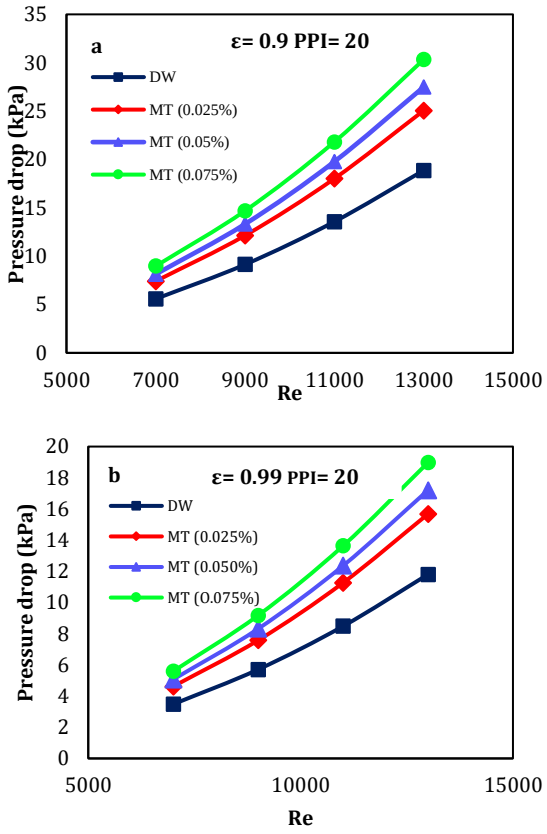

Figure 9. Pressure drop as function of Re number for different nanofluids mass fraction and for 20 PPI and: (a) ε = 0.9, (b) ε = 0.99.

Figure 10 illustrates the Nua (average Nusselt number) of the channel with metal foam for different mass fractions of nanofluids, considering two values of porosity and a pore density of 20 PPI. As the Reynolds number increases, the Nua increases for both porosity values and all nanofluids. The Nua of metal foam with a porosity of 0.9 is higher than that of metal foam with a porosity of 0.99 due to the stronger influence of thermal conductivity in the former. Furthermore, the heat transfer enhancement in metal foam with a porosity of 0.9 is 9.8% greater than in metal foam with a porosity of 0.99. In all cases, the Nua of MT (0.075%) is higher than in the other scenarios due to its higher viscosity.

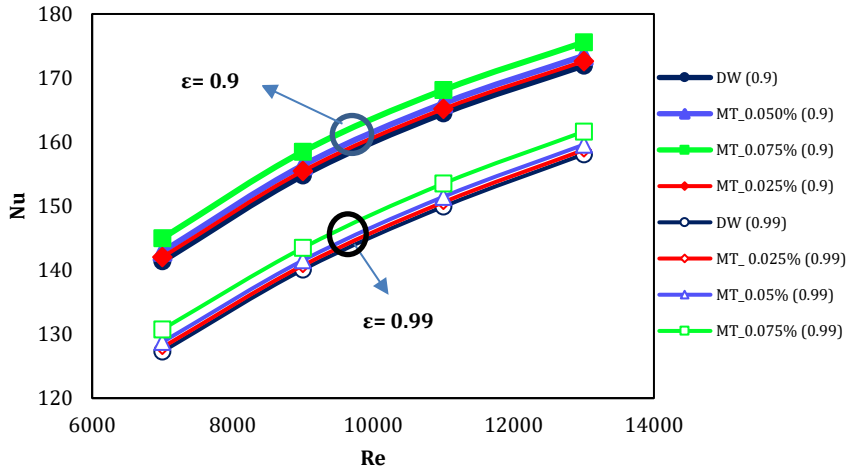

Figure 10. Nu_a as function of Re number for different nanofluids mass fraction and for 20 PPI, ε = 0.9 and ε = 0.99

Figure 11 presents the Nua as a function of porosity for different nanofluid mass fractions, with a pore density of 20 PPI, and at two Reynolds numbers of 7000 and 13000, respectively. As the porosity of the metal foam increases, the Nua decreases for all nanofluids. This decrease is attributed to the diminishing effect of thermal conductivity in the metal foam as porosity increases.

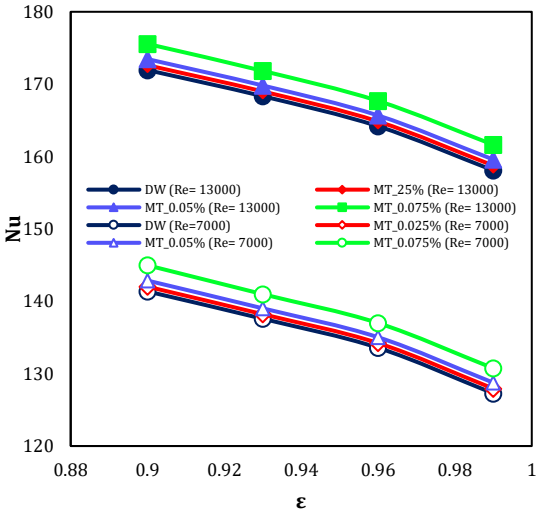

Figure 11. Nu_a as function of porosity for different nanofluids mass fraction and for 20 PPI, Re= 7000 and Re = 13000

Figure 12 illustrates the impact of porosity and pore density of metal foam on thermal performance when using distillate water fluid (without nanofluids). In Figure 12(a) and Figure 12(b), the Nua is presented as a function of porosity, pore density, and Reynolds numbers of 7000 and 13000. In both cases, when porosity decreases and pore density increases, the Nua increases. Furthermore, the maximum Nua reaches 181 when Reynolds is 7000 and 203 when Reynolds is 13000.

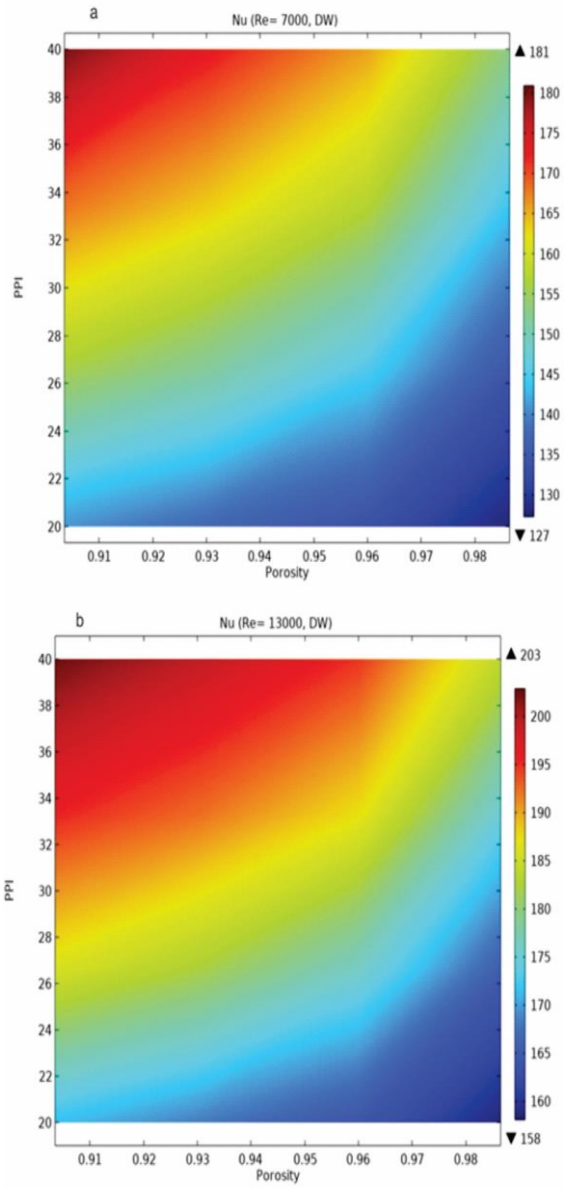

Figure 12. AN as function of porosity and pore density for a: Re= 7000, b: Re = 13000

Figure 13 shows the effect of porosity and Re number with distillate water fluid (without nanofluids) on thermal performance. In Figure 13 (a) and Figure 13 (b), the Nua as function of porosity, Reynolds number and pore density equal to 20 and 40 are shown. In both cases, if the porosity decreases and the Re number increases, the Nua increase. Also, the maximum of the Nua is equal to 172 when PPI is 20 and equal to 203 when PPI is 40.

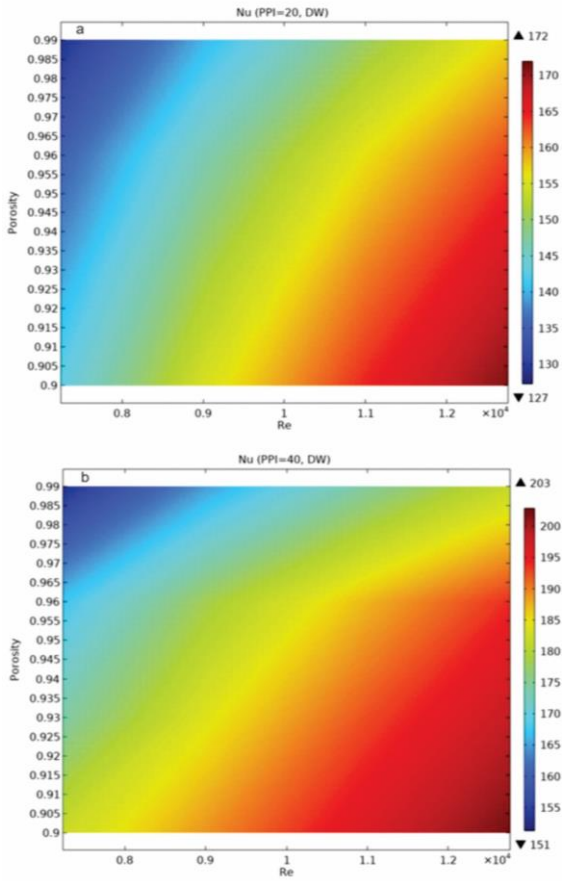

Figure 13. ANu as function of porosity and Re number for a: PPI= 20, b: PPI = 40

Figure 14 illustrates the impact of pore density (PPI) and Reynolds number, using distillate water fluid (without nanofluids), on thermal performance. In both Figure 14(a) and Figure 14(b), the Nu_a is presented as a function of PPI, Reynolds number, and porosity, with values equal to 0.9 and 0.99. In both cases, when the Reynolds number and PPI increase, the Nusselt number also increases. Additionally, the maximum Nu_a reaches 172 when the porosity is 0.99 and increases to 203 when the porosity is 0.9.

Figure 15 shows the effect of porosity and pore density of metal foam with MT (0.075 %) nanofluid on thermal performance. In Figure 15 (a) and Figure 15 (b), the Nua as function of porosity, pore density and Reynolds number 7000 and 13000 are shown. In both cases, if the porosity decreases and the pore density increases, the Nua increase. Also, the maximum of the Nua is equal to 185 when Reynolds is 7000 and equal to 207 when Reynolds is 13000.

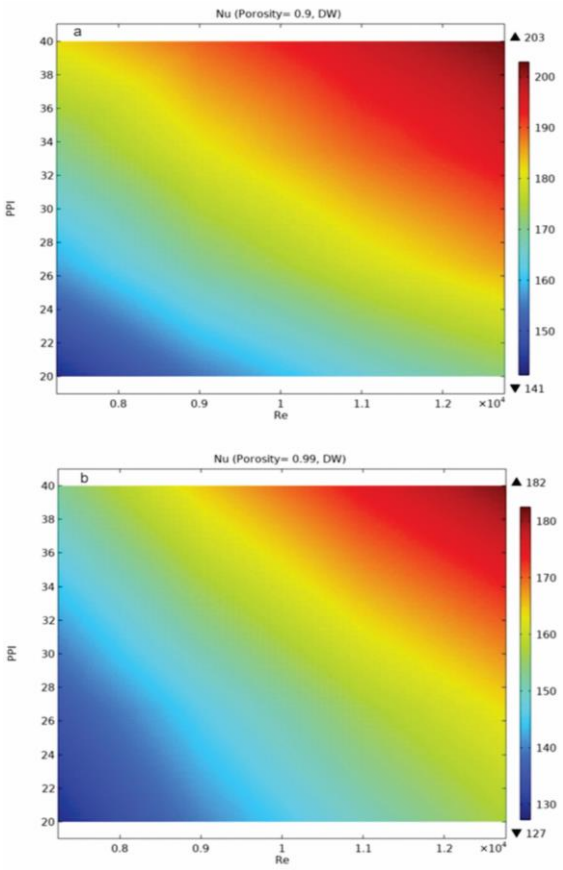

Figure 14. Nu_a as function of PPI and Re number for a: porosity= 0.9, b: porosity = 0.99

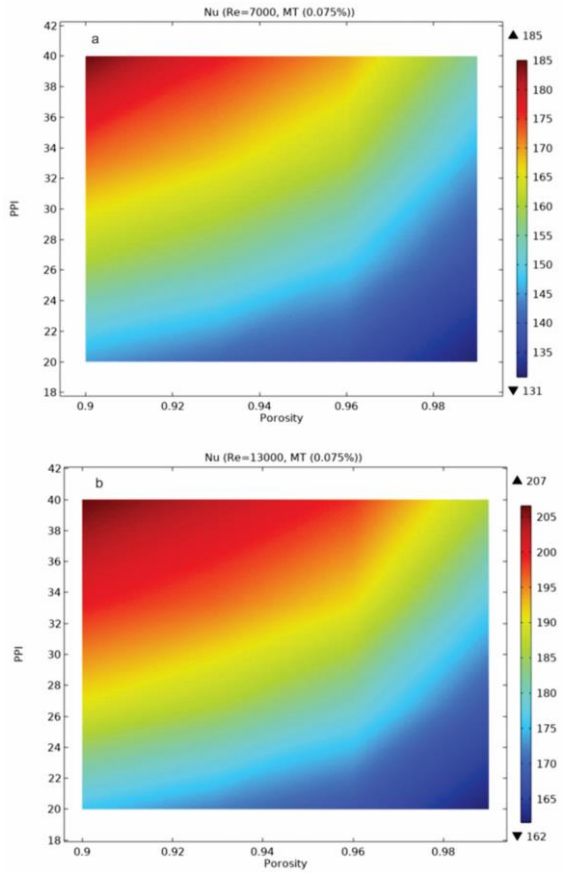

Figure 15. Nua as function of porosity and pore density for MT (0.075%) a: Re= 7000, b: Re = 13000

Figure 16 illustrates the impact of porosity and Reynolds number using MT (0.075%) nanofluids on thermal performance. In both Figure 16(a) and Figure 16(b), the Nua is presented as a function of porosity, Reynolds number, and pore density, with values equal to 20 and 40. In both cases, when porosity decreases and the Reynolds number increases, the Nua also increases. Additionally, the maximum Nua reaches 176 when PPI is 20 and increases to 207 when PPI is 40.

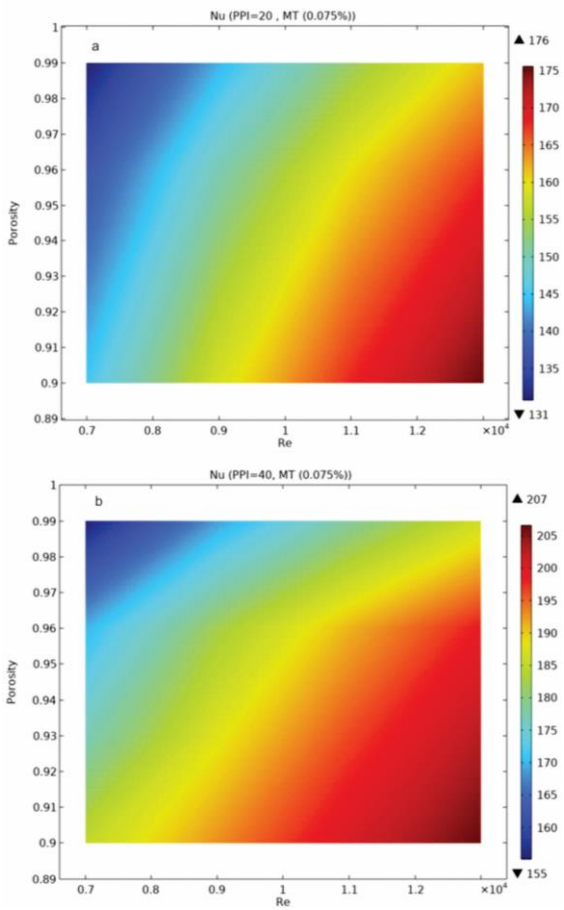

Figure 16. Nu_a as function of porosity and Re number for MT (0.075%) a: PPI= 20, b: PPI = 40

Figure 17 illustrates the impact of pore density (PPI) and Reynolds number using MT (0.075%) nanofluid on thermal performance. In both Figure 17(a) and Figure 17(b), the Nua is presented as a function of PPI, Reynolds number, and porosity, with values equal to 0.9 and 0.99. In both cases, when the Reynolds number and PPI increase, the Nua also increases. Additionally, the maximum Nua reaches 186 when porosity is 0.99 and increases to 207 when porosity is 0.9.

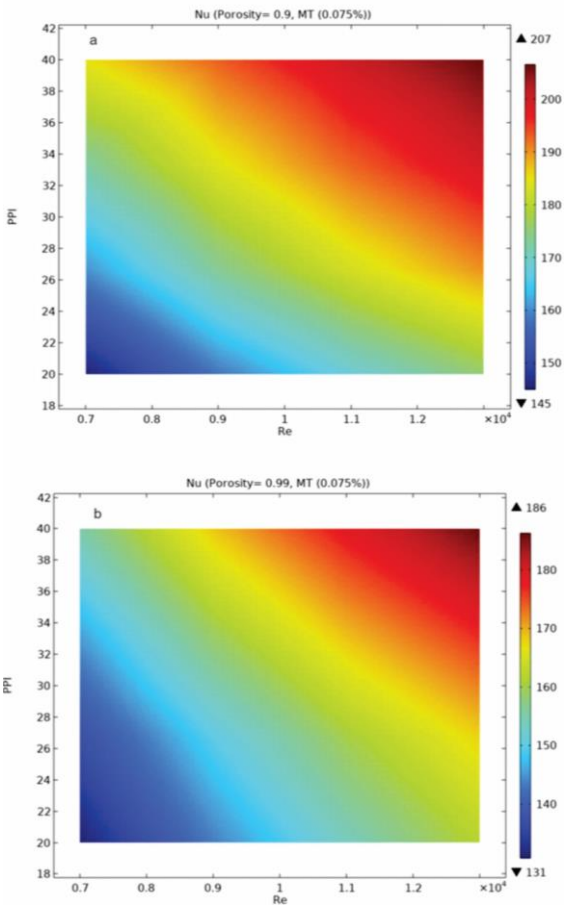

Figure 17. Nu_a as function of PPI and Re number for MT (0.075 %) a: porosity= 0.9, b: porosity = 0.99

In Table 4, the predicted correlation coefficients for Nua as a function of Reynolds number, porosity, and pore density are presented for all hybrid nanofluids. The values of R-square, which are close to one, indicate that the predictions are in agreement with the data. Figure 18 displays the estimated Nua values alongside the actual values for all nanofluids.

Table 4. The predicted correlation coefficients for Nu_a

$$Nu = a + bx + cy + dz + exy + fxz + gyz + hx^2 + iy^2 + jz^2$$
$$x = Re, y = Porosity, z = PPI$$

Hybrid nanofluid	a	b	c	d	e	f	g	h	i	j	R^2
DW	-1585	0.006	3551	7.47	0.006	0	-4.8	-3.14	-1959	-0.01	0.99
MT (0.025 %)	-1587	0.006	3558	7.47	0.006	0	-4.8	-3.15	-1964	-0.01	0.99
MT (0.05 %)	-1591	0.006	3568	7.5	0.006	0	-4.8	-3.16	-1970	-0.01	0.99
MT (0.075 %)	-1595	0.006	3585	7.5	0.006	0	-4.8	-3.17	-19.81	-0.01	0.99

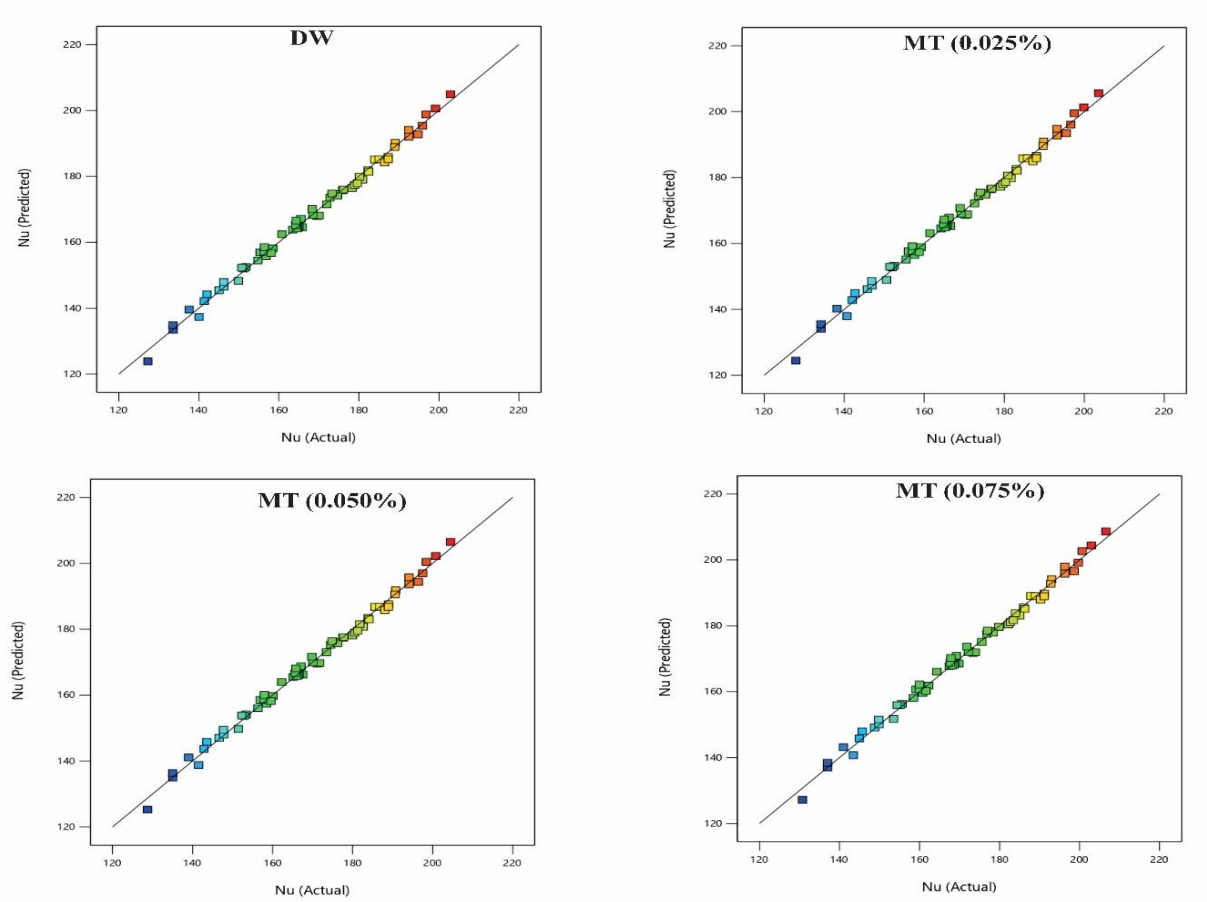

Figure 18. Predicted and actual Nu_a

Table 5 presents the optimal values of Nua along with the associated optimal parameters. In these optimal conditions, the Nua of MT (0.075%) is 2.4% higher than that of DW (without nanofluids).

Table 5. The optimal values of Nu_a for all nanofluids

Hybrid nanofluid	Optimal values of the average Nusselt number	Porosity	Re	PPI
DW	202	0.910	12826	39.6
MT (0.025%)	203	0.905	12540	39.8
MT (0.050%)	205	0.908	12858	39.7
MT (0.075%)	207	0.908	12839	39.6

Conclusions

In this research, modeling and simulation of hybrid nanofluids (MWCNTs+TiO2) with DW (distilled water) as the base fluid were performed in a channel with triangular corrugations and open metal foam. The flows of the hybrid nanofluids were assumed to be turbulent (with higher Reynolds numbers), steady-state, two-dimensional, Newtonian, incompressible, and single-phase. The mass fractions of hybrid nanofluids (a mixture of DW and MWCNTs+TiO2) were set at 0.025%, 0.05%, and 0.075%. The effects of metal foam porosity and PPI (pore density) at two different Reynolds numbers (7000-13000) on thermal performance were investigated. The results showed that heat transfer with metal foam increased by 130% for all hybrid nanofluids. The enhancement of heat transfer using metal foam with a porosity of 0.9 was 9.8% greater than with metal foam with a porosity of 0.99. Additionally, quadratic correlations for Nua for all hybrid nanofluids, considering PPI, porosity, and Reynolds numbers as variables, were proposed. The values of R-square, which were close to one, indicated that the predictions were in agreement with the data. Finally, the optimum values of Nua for all hybrid nanofluids were determined. In optimal conditions, Nua for MT (0.075%), MT (0.05%), MT (0.025%), and DW were determined to be 207, 205, 203, and 202, respectively.

Nomenclature

a	Nanofluids specific surface area density (1/m)
c_p	Specific heat capacity (J/kg K)
C_ε	Parameters of turbulence (k-ε) (1)
d	Hydraulic diameter (m)
d_f	Diameter of fiber (m)

d_p Diameter of pore (m)

h Interfacial heat transfer coefficient (W/m2K)

k Turbulent kinetic energy (m2/s2)

k_{nf} Thermal conductivity of nanofluids (W/m K)

k_s Thermal conductivity of solid (W/m K)

Nu Nusselt number (1)

p Pressure (Pa)

Pr Prandtl number (1)

q'' Heat flux (W/m2)

Re Reynolds number (1)

T Temperature (K)

u Vector of velocity ([u, v]) (m/s)

Greek symbols

ε Turbulent dissipation rate (m2/s3)

ε_p Porosity of metal foam (1)

κ Permeability (1/m2)

μ Viscosity (Pa. s)

ρ Density (kg/m3)

Subscripts

b Bulk

n_f Nanofluids

S Solid

Nu_a Average Nusselt number

MT MWCNTs+TiO2

Conflicts of Interest

The author declares that there is no conflict of interest regarding the publication of this manuscript. In addition, the authors have entirely observed the ethical issues, including plagiarism, informed consent, misconduct, data fabrication and/or falsification, double publication and/or submission, and redundancy.

References

[1] Sheng Bu, C., Yin Liu, D., Ping Chen, X., Liang, C., Feng Duan, Y., Bo Duan, L., 2013. Modeling and Coupling Particle Scale Heat Transfer with DEM through Heat Transfer Mechanisms. Numerical Heat Transfer, Part A: Applications, 64(1), pp. 56-71.

[2] Meyer, J. P., 2013. Heat Transfer, Fluid Mechanics and Thermodynamics—HEFAT2011. Heat Transfer Engineering, 34(14), pp. 1141-1146.

[3] Kim, J. S., Park, B. K., Lee, J. S., 2009. Natural Convection Heat Transfer Around Microfin Arrays. Experimental Heat Transfer, 21(1), pp. 55-72.

[4] Wang, H., Guo, L., 2019. Volumetric Convective Heat Transfer Coefficient Model for Metal Foams. Heat Transfer Engineering, 40(5-6), pp. 464-475.

[5] Leong, K. C., Jin, L. W., 2006. Effect of oscillatory frequency on heat transfer in metal foam heat sinks of various pore densities. International Journal of Heat and Mass Transfer, 49(3-4), pp. 671-681.

[6] Lua, W., Zhaoab, C. Y., Tassoua, S. A., 2006. Thermal analysis on metal-foam filled heat exchangers. Part I: Metal-foam filled pipes. International Journal of Heat and Mass Transfer, 49(15-16), pp. 2751-2761.

[7] Yu, Q., Straatmana, A. G., Thompsonb, B. E., 2006. Carbon-foam finned tubes in air–water heat exchangers. Applied Thermal Engineering, 26(2-3), pp. 131-143.

[8] Laurencelle, F., Goyette, J., 2007. Simulation of heat transfer in a metal hydride reactor with aluminium foam. International Journal of Hydrogen Energy, 32(14), pp. 2957-2964.

[9] Du, Y. P., Qua, Z. G., Zhao, C. Y., Tao, W. Q., 2010. Numerical study of conjugated heat transfer in metal foam filled double-pipe. International Journal of Heat and Mass Transfer, 53(21-22), pp. 4899-4907.

[10] Khadangi, M., Etemad, M., Bagheri, R., 2011. Free convection heat transfer of non-Newtonian nanofluids under constant heat flux condition. International Communications in Heat and Mass Transfer, 38(10), pp. 1449-1454.

[11] Su, F., Ma, X., Lan, Z., 2011. The effect of carbon nanotubes on the physical properties of a binary nanofluid. Journal of the Taiwan Institute of Chemical Engineers, 42(2), pp. 252-257.

[12] Yu, L., Liu, D., Botz, F., 2012. Laminar convective heat transfer of alumina-polyalphaolefin nanofluids containing spherical and non-spherical nanoparticles. Experimental Thermal and Fluid Science, 37, pp. 72-83.

[13] PERARASU, V. T., ARIVAZHAGAN, M., SIVASHANMUGAM, P., 2012. Heat transfer of TiO2/water nanofluid in a coiled agitated vessel

with propeller. Journal of Hydrodynamics, Ser. B, 24(6), pp. 942-950.

[14] Ijam, A., Saidur, R., 2012. Nanofluid as a coolant for electronic devices (cooling of electronic devices). Applied Thermal Engineering, 32, pp. 76-82.

[15] Wang, P. Y., Chen, X. J., Liu, Z. H., Liu, Y. P., 2012. Application of nanofluid in an inclined mesh wicked heat pipes. Thermochimica Acta, 539, pp. 100-108.

[16] Bai, C., Wang, L., 2013. Two nanofluid configurations for heat conduction systems: performance comparison. International Journal of Heat and Mass Transfer, 66, pp. 632-642.

[17] Shaha, J., Kumarb, S., Ranjanc, M., Sonvanea, Y., Tharejab, P., Guptad, S. K., 2018. The effect of filler geometry on thermo-optical and rheological properties of CuO nanofluid. Journal of Molecular Liquids, 272, pp. 668-675.

[18] Rekhaa, M. B., Sarrisb, I. E., Madhukesh, J. K., Raghunatha, K. R., Prasannakumaraa, B. C., 2022. Impact of Thermophoretic particle deposition on heat transfer and nanofluid flow through different geometries: an application to solar energy. Chinese Journal of Physics, 2022, 1921.

[19] Gariaa, R., Rawatb, S. K., Kumara, M., Yaseena, M., 2021. Hybrid nanofluid flow over two different geometries with Cattaneo–Christov heat flux model and heat generation: A model with correlation coefficient and probable error. Chinese Journal of Physics, 74, 2021, pp. 421-439.

[20] Hamida, M. B. B., Hatamid, M., 2021. Investigation of heated fins geometries on the heat transfer of a channel filled by hybrid nanofluids under the electric field. Case Studies in Thermal Engineering, 28, 101450.

[21] Zachár, A., 2010. Analysis of coiled-tube heat exchangers to improve heat transfer rate with spirally corrugated wall. International Journal of Heat and Mass Transfer, 53(19-20), pp. 3928-3939.

[22] Hekmat, M., Saharkhiz, S., 2022. Effect of Nanofluid Flows on Heat Transfer Intensification of Corrugated Channels with an Oscillating Blade. Chemical Engineering and Processing - Process Intensification, 179, 109072.

[23] Zahrana, S., Sultan, A. A., Bekheit, M., Elmarghany, M. R., 2022. Heat transfer augmentation through rectangular cross section duct with one corrugated surface: An experimental and numerical study. Case Studies in Thermal Engineering, 36, 102252.

[24] Obaidia, A. R. A., Alhamid, J., AliKhalaf, H., 2022. Effect of different corrugation interruptions Parameters on thermohydrodynamic characteristics and heat transfer performance of 3D Three-dimensional corrugated tube. Case Studies in Thermal Engineering, 32, 101879.

[25] Amar, Z., Rabinovich, E., Baroukh, I., Ziskinda, G., 2022. Parametric study of heat transfer coefficient and friction factor in a corrugated channel. International Journal of Heat and Mass Transfer, 196, 123290.

[26] Feng, C. N., Liang, C. H., Li, Z. X., 2022. Friction factor and heat transfer evaluation of cross-corrugated triangular flow channels with trapezoidal baffles. Energy and Buildings, 257, 111816.

[27] Li, X. J., Tan, X. M., Zhang, J. Z., Wu, B. B., Chena, W. W., 2022. Utilizing piezoelectric fan for heat transfer enhancement on corrugated surfaces. Thermal Science and Engineering Progress, (29), 101219.

[28] Lia, Y., Yu, Q., Yu, S., Gonga, B., Zhang, J., 2022. Numerical investigation of pulsating flow structures and heat transfer enhancement performance in spherical corrugated helical tube. Applied Thermal Engineering, 213, 118647.

[29] Talib, A. R. A., Hiloa, A. K., 2021. Fluid flow and heat transfer over corrugated backward facing step channel. Case Studies in Thermal Engineering, 24, 100862.

[30] Hu, Q., Qu, X., Peng, W., Wang, J., 2022. Experimental and numerical investigation of turbulent heat transfer enhancement of an intermediate heat exchanger using corrugated tubes. International Journal of Heat and Mass Transfer, 185, 122385.

[31] Li, W., Zhang, L., Klemešc, J. J., Wanga, Q., Zeng, M., 2022. Thermochemical energy conversion behaviour in the corrugated heat storage unit with porous metal support. Energy, In Press, Journal Pre-proof (2022), 124966.

[32] Bianco, V., Buonomo, B., di. Pasqua, A., Manca, O., 2021. Heat transfer enhancement of laminar impinging slot jets by nanofluids and metal foams. Thermal Science and Engineering Progress, (2021), 100860.

[33] Wan, Y., Wu, R., Qi, C., Duan, G., Yang, R., 2018. Experimental study on thermo-hydraulic performances of nanofluids flowing through a corrugated tube filled with copper foam in heat exchange systems. Chinese Journal of Chemical Engineering, Volume 26(12), pp. 2431-2440.

[34] Alawi, O. A., Kamar, H. M., Hussein, O. A., Mallah, A. R., Mohammed, H. A., Khiadani, M., Roomi, A. B., Kazi, S. N., Yaseen, Z. M., 2022. Effects of binary hybrid nanofluid on heat transfer and fluid flow in a triangular-corrugated channel: An experimental and numerical study. Powder Technology, 395, pp. 267–279.

[35] COMSOL Group, 2021. COMSOL Multiphysics (V.6). https://www.comsol.com

[36] Xiao, T., Liu, G., Guo, J., Shu, G., Lu, L., Yang, X., 2022. Effect of metal foam on improving solid–liquid phase change in a multi-channel thermal storage tank. Sustainable Energy Technologies and Assessments, 53, 102533.